J Mater Sci: Mater Electron (2022) 33:10297–10313

Growth mechanisms of intermetallic compounds and Bi-rich layer in ball grid array structure Cu/Sn-58Bi/Cu solder joints during solid–solid and liquid–solid electromigration

Jiaqiang Huang[1,2,*] , Xudong Wang[2], Junyu Chen[2], Weichun Wei[2], Fengmei Liu[1], Binhao Qin[1], Haiyan Wang[1,*], and Yupeng Zhang[1]

[1] *China-Ukraine Institute of Welding, Guangdong Provincial Key Laboratory of Advanced Welding Technology, Guangdong Academy of Sciences, Guangzhou 510650, China*

[2] *School of Mechanical and Electrical Engineering, Guilin University of Electronic Technology, Guilin 541004, China*

Received: 5 January 2022

Accepted: 28 February 2022

Published online: 1 April 2022

© The Author(s), under exclusive licence to Springer Science+Business Media, LLC, part of Springer Nature 2022

ABSTRACT

Sn-58Bi solder has attracted much attention due to its low melting temperature and low cost in recent years. However, Sn-58Bi solder might occur locally melting due to the high local temperature by Joule heating and consequently raises serious reliability problems. In this study, the growth mechanisms of interfacial intermetallic compounds (IMCs) and Bi-rich layer of the ball grid array structure Cu/Sn-58Bi/Cu joints during both solid–solid (S–S) electromigration in solid solder and liquid–solid (L–S) electromigration in molten solder were investigated comprehensively. Results show that during S–S electromigration at 70 °C, current stressing induces a reverse polarity effect on the growth of interfacial IMCs, i.e., the interfacial IMCs on the cathode side is thicker than that on the anode side. Besides, Bi atoms accumulate to form a Bi-rich layer on the anode side. During S–S electromigration at 135 °C, current stressing causes a reverse polarity effect on the growth of interfacial IMCs, and Bi atoms on the anode side reversely diffuse into the solder, resulting in the disappearance of Bi-rich layer. During L–S electromigration at both 150 °C and 170 °C, current stressing induces a polarity effect on the growth of interfacial IMCs, i.e., the interfacial IMCs on the anode side is thicker than that on the cathode side. Furthermore, there is no Bi-rich layer on the anode side. The transition in growth mechanism of interfacial IMCs from the reverse polarity effect to the polarity effect is determined by the combined effect of the electronic wind force flux (J_{em}) and the chemical potential gradient flux (J_{chem}).

Address correspondence to E-mail: huangjiaqiang201@163.com; wanghy@gwi.gd.cn

https://doi.org/10.1007/s10854-022-08018-x

1 Introduction

In the past two decades, the ball grid array (BGA) technology has been a preferable assembly selection for high-density and low-cost packaging in electronic packaging [1]. Nowadays, Sn–Ag–Cu solders, as one of the mainstream lead-free solders, have been widely used in BGA packaging. Nevertheless, its high Ag content not only increases the cost of solder but also leads to the formation of bulk Ag_3Sn, which weakens the mechanical properties of the solder joints [2, 3]. Besides, its high melting temperature (217 to 227 °C) may causes thermal damage of electronic components [4]. In recent years, with the increasing demand for low-cost or low-temperature reflow processes in the electronics industry, the characteristics of high cost and high melting temperature limit the further application of Sn–Ag–Cu solders. Therefore, the binary eutectic Sn-58Bi solder has been gradually attracted much attention due to features of low cost, low melting temperature (138 °C), and high tensile strength [5–8].

In recent years, with continuous miniaturization and multi-performance of electronic products, the size of solder joint is decreased significantly [9]. As a result, the current density passing through the solder joint increases dramatically, inducing severe electromigration phenomenon [10]. During electromigration, the high current density could increase the operating temperature of solder joint due to the effect of Joule heating, and even results in the local melting of the solder joint, especially for low melting-point Sn-58Bi solder joint, which leads to the transformation of solid–solid (S–S) electromigration into liquid–solid (L–S) electromigration [11, 12]. The S–S electromigration refers to the physical states of the solder and substrate are all solids, and the L–S electromigration refers to the physical state of solder is liquid, while that of the substrate is solid. Owing to the surface tension and the protection of the polymer filler, the solder joint maintains its initial shape even after melting and works temporarily normally until the substrate, i.e., the under bump metallization (UBM), is completely consumed [13].

During S–S electromigration in solid Sn-58Bi solder, mass transport of atomic flux occurs under the force of electron flow, which promotes the growth of interfacial intermetallic compounds (IMCs) on the cathode side and the formation of Bi-rich layer on the anode side [14]. The formation of interfacial IMCs is a crucial factor for the good metallurgical bonding between the solder and substrate. However, owing to the natural brittleness of the IMC phase, massive IMCs may degrade the mechanical properties of the solder joints and act as initiation sites for micro-cracks, resulting in interfacial failures between the solder and substrate [15, 16]. Meanwhile, Bi-rich layer not only increases the electrical resistance of Sn-58Bi solder joints, but also reduces the plasticity of solder and leads to brittle fracture of solder joints [17, 18]. Therefore, in the past decade, numerous studies have been conducted to investigate the growth mechanisms of interfacial IMCs and Bi-rich layer in solder joints during electromigration [19–21].

However, to date, most studies to growth mechanisms of interfacial IMCs and Bi-rich layer have focused mainly on S–S electromigration in solid Sn-58Bi solder, and rarely on the L–S electromigration in molten Sn-58Bi solder. In fact, since the diffusivity of atoms in liquid is significantly higher than that in solid, the interfacial IMCs evolution and atomic diffusion behaviors of solder joints under L–S electromigration should be greatly different from that under S–S electromigration, which have been verified by previous studies. For example, Huang et al. [22] studied the electromigration behavior in molten Sn-3.5Ag solder, and found that the Cu atoms from the cathode side were driven to the anode side to form a thick Cu_6Sn_5 layer. Ma et al. [23] reported the thickness of interfacial Cu_6Sn_5 on the anode side could be obtained as 110 μm in Cu/Sn/Cu joint undergoing L–S electromigration. Zhang et al. [24] investigated the diffusion behaviors of atoms and interfacial reaction in molten Sn-52In solder, and found that the In atoms migrated toward the anode side and contributed to the polarity effect in the growth of interfacial IMCs during L–S electromigration, which is different from the In atoms migrated toward the cathode side during S–S electromigration. Li et al. [25] found that the growth rate of interfacial IMC in molten Sn-3.0Ag-0.5Cu solder during electromigration is higher than those in the solid state solder joints. Thus, it is particularly important to study the growth mechanisms of interfacial IMCs and Bi-rich layer during L–S electromigration in molten Sn-58Bi solder. In addition, in order to deeply clarify the mechanisms of interfacial IMCs evolution and Bi atomic diffusion behaviors during L–S electromigration, it is also necessary to investigate the growth mechanisms of interfacial IMCs and Bi-rich layer

during S–S electromigration in solid Sn-58Bi solder with the increasing temperature.

In this study, an in-depth and systematic study of growth mechanisms of interfacial IMCs and Bi-rich layer in BGA structure Cu/Sn-58Bi/Cu solder joints during S–S and L–S electromigration is reported, which aims at enriching our understanding of atomic diffusion behaviors of the Sn-58Bi solder joints with the increasing temperature, and providing useful guidance for design of micro interconnection and reliability evaluation of the solder joints.

2 Experimental procedures

In this study, a single BGA structure solder joint was designed, in which Cu pad with a diameter of 320 μm, Sn-58Bi solder ball with a diameter of 450 μm were used to prepare joint samples. Firstly, Cu pad on PCB was reflowed with Sn-58Bi solder ball to form a single-sided IC package with BGA pin. Afterward, the single-sided sample with BGA pin was flipped and mounted onto the surface of Cu pad on another PCB, and then the mounted sample was reflowed to form a BGA structure Cu/Sn-58Bi/Cu joint using a typical temperature curve with the peak temperature of 195 °C and duration of 80 s above the melting temperature (138 °C) of the Sn-58Bi solder. A schematic illustration of the designed joint is shown in Fig. 1.

The electromigration test was performed by a DC power supply, and the direction of electron flow is from the top right corner to bottom left corner of joint sample. In order to ensure the shape of the solder is not damaged during electromigration test, each joint sample was enchased and encapsulated in resin. During S–S electromigration test, the joint samples were divided into two groups, one group was subjected to current stressing with a density of 1.0×10^4 A/cm^2 at 70 °C for different dwelling times of 0, 25, 50, 100, and 200 h, respectively. The other was subjected to current stressing with a density of 1.0×10^4 A/cm^2 at 135 °C for different dwelling times of 0, 6, 12, 18, and 25 h, respectively. During L–S electromigration test, the joint samples were divided into three groups, one group was subjected to current stressing with a density of 1.0×10^4 A/cm^2 at 150 °C for different dwelling times of 0, 6, 12, 18, and 25 h, respectively, another one was subjected to current stressing with higher density of 1.5×10^4 A/cm^2 at 150 °C for different dwelling times of 0, 6, 12, 18, and 25 h, respectively, the final group was subjected to current stressing with a density of 1.0×10^4 A/cm^2 at 170 °C for different dwelling times of 0, 6, 12, 18, and 25 h, respectively.

Since the Joule heating will generate most of heat in joint samples, in order to ensure the electromigration test is performed in a constant temperature, the joint samples were put into the silicone oil and were subjected to current stressing, as a result, the real temperature of joint samples is determined by the

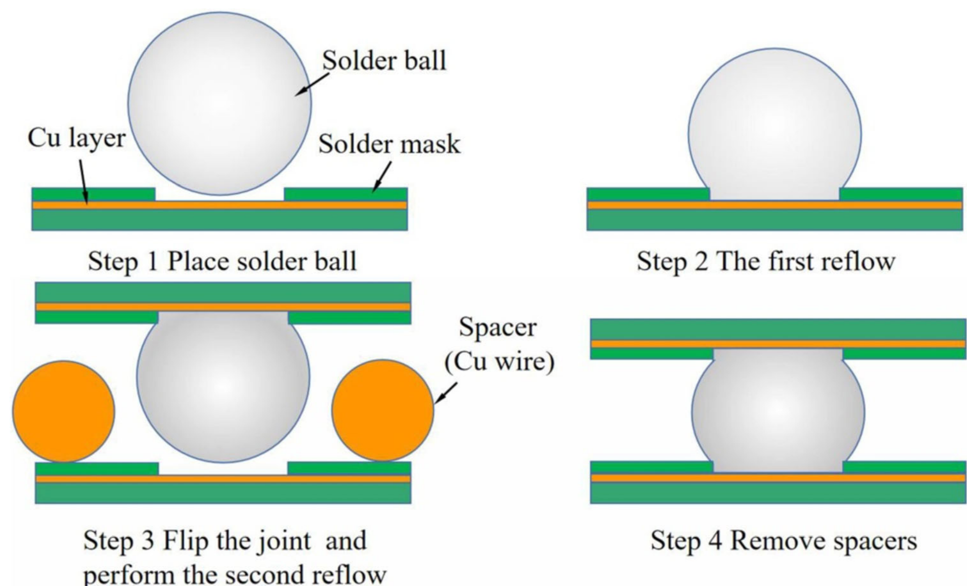

Fig. 1 Schematic diagram of preparation process of BGA structure Cu/Sn-58Bi/Cu joint

coupling effect of Joule heating and oil temperature. A schematic diagram of the electromigration test equipment and solder joint is illustrated in Fig. 2. To monitor the real temperature of joint samples accurately, a thermocouple with a tip size of 80 μm was attached on the surface of the joint, and then they were enchased in resin and subjected to current stressing. Because of the protection of resin, and the tip size of the thermocouple was much smaller than the diameter of solder ball, the thermocouple does not damage the solder joint structure, even though when the temperature exceeds the melting point of solder during L–S electromigration test. The results showed that after electromigration with a current density of 1.0×10^4 A/cm^2 at oil temperature of 55 °C, 120, 130 and 140 °C for 1 min, respectively, the real temperature of joint sample increased rapidly and then reached a stable value of 70 ± 1, 135 ± 1, 150 ± 1, and 170 ± 1 °C, respectively, while after electromigration with a current density of 1.5×10^4 A/cm^2 at oil temperature of 100 °C for 1 min, the real temperature of joint sample increased rapidly and then reached a stable value of 150 ± 1 °C. In addition, three identical solder joint samples were tested under each of five stressing time in each group so as to have reliable data and perform the statistical analysis.

After electromigration test, the joints samples were ground along the cross-sectional plane using a series of SiC sandpapers, and subsequently polished with Al_2O_3 suspension and finally etched by a mixed solution of $2\%HNO_3 + 3\%HCl + 95\%C_2H_5OH$ (vol.%). The composition of the interfacial IMCs and the microstructure of the solder joints were analyzed by a scanning electron microscope (SEM, FEI, Quanta 450, USA) equipped with an energy dispersive spectrometer (EDS, X-Max20, Oxford Instruments). To study the growth behavior of the interfacial IMCs layer in joints, the values of the average thickness of the interfacial IMCs layer of the joints on each condition were obtained by measurement using SEM, that is, the cross-sectional microstructure of the interfacial IMCs layer from different position of the joint was observed and recorded for three times by SEM, and the integrated area and length of the IMCs layer in the joint were obtained using image analysis software, and then the average thickness of the interfacial IMCs layer was determined by dividing the integrated area by the length of the IMC layer, the detailed measurement method could be obtained by reference to the previous study [26].

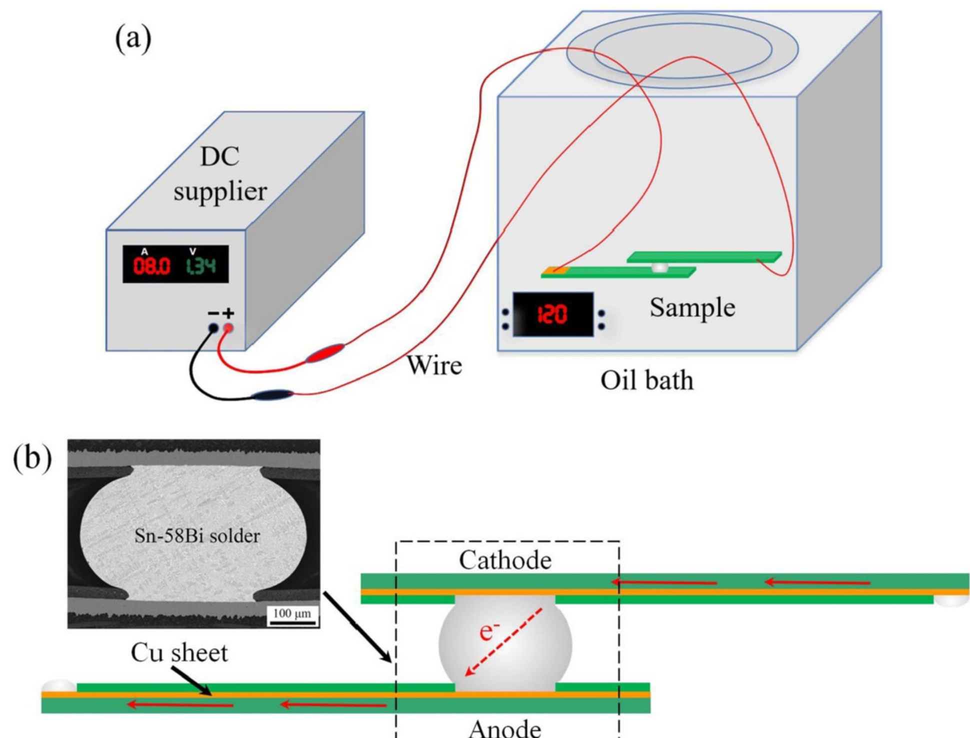

Fig. 2 Schematic diagram of the electromigration test: **a** 3-D diagram of the electromigration with equipment, **b** the 2-D simple structure

3 Results and discussion

3.1 Microstructure of the as-reflowed joint

Figure 3 shows the cross-sectional microstructure of the as-reflowed BGA structure Cu/Sn-58Bi/Cu joint. Clearly, the microstructure of the eutectic solder is consisted of gray Sn-rich phases and white Bi-rich phases. Moreover, a very thin scallop-type IMC layer, which is identified as Cu_6Sn_5 by EDS analysis, forms at the interface between the Sn-58Bi solder and Cu substrate, as shown in Fig. 3b, c. The interfacial Cu_6Sn_5 is the reaction product of Sn atoms from Sn-58Bi solder and Cu atoms from Cu substrate, which can realize the metallurgical bonding.

3.2 The microstructural evolution of solder joints during S–S electromigration

Figure 4 shows the cross-sectional microstructures of BGA structure Cu/Sn-58Bi/Cu joints after S–S electromigration with the current density of 1.0 × 10^4 A/cm^2 at 70 °C for different times, where the red arrow labeled with the symbol e^- indicates the direction of electron flow, and the top interface and bottom interface of the solder joint represent the cathode side and anode side, respectively. During S–S electromigration at 70 °C, which the temperature is much lower than the melting temperature of Sn-58Bi solder, the solder remains the original solid state. After current stressing for 25 h, as shown in Fig. 4a–c, the thickness of interfacial scallop-type Cu_6Sn_5 layer increases obviously, and a very thin planar-type Cu_3Sn layer forms at the interface between the Cu_6Sn_5 layer and Cu substrate, which the compositions of the Cu_6Sn_5 and Cu_3Sn are confirmed by the results of EDS analysis in Fig. 5. Therefore, the interfacial IMCs of solder joint is consist of Cu_6Sn_5 and Cu_3Sn layer, and the thicknesses of the interfacial IMCs on both the cathode and anode sides are about 7.85 µm and 3.39 µm, respectively, where the thickness near the top right corner is much thicker than that near the top left corner. Besides, a continuous Bi-rich layer is observed on the anode side, resulting from Bi atomic migration and segregation under the driving force of electronic wind. The result on the formation of Bi-rich layer on the anode side during S–S electromigration is similar with the finding in the previous study [14]. Unfortunately, due to the inherent brittleness and the higher resistivity of Bi, the Bi-rich layer may lead to the strength reduction and the more serious Joule heating at the joint interface [27–29]. As the current stressing time increases to 50 h, as depicted in Fig. 4d–f, the thicknesses of the interfacial IMCs on both the cathode and anode sides increase to 8.60 µm and 4.27 µm, respectively. Moreover, the thickness of the Bi-rich layer increases. When the current stressing time further increases to 100 h, as shown in Fig. 4g–i, there is no obviously change in the thickness of the interfacial IMCs, while the Bi-rich layer becomes thicker. When the current stressing time increases to 200 h, as shown in Fig. 4j–l, the thickness of the interfacial IMCs on the cathode side increases significantly to 25.93 µm, while that on the anode side increases to 7.81 µm.

In order to clarify the effect of the temperature on the interfacial reaction and Bi atomic migration in solid solder, we carried out the S–S electromigration at 135 °C, which the current density is 1.0 × 10^4 A/cm^2 and the temperature is slightly lower than the melting temperature of Sn-58Bi solder, and the results are shown in Fig. 6. Obviously, after current stressing for 6 h, as shown in Fig. 6a–c, a planar Cu_3Sn layer forms at the interface between the Cu_6Sn_5 layer and Cu substrate, and the thicknesses of the

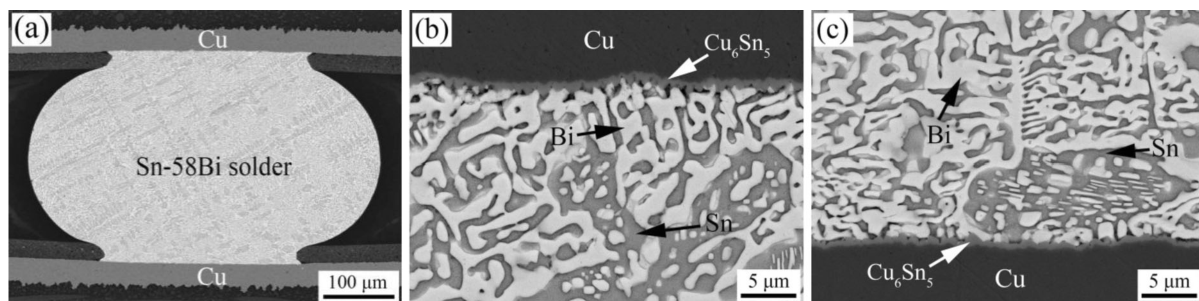

Fig. 3 Cross-sectional microstructure of the as-reflowed BGA structure Cu/Sn-58Bi/Cu joint: **a** the solder joint, **b** the top interface region in (**a**), **c** the bottom interface region in (**a**)

Fig. 4 Cross-sectional microstructures of BGA structure Cu/Sn-58Bi/Cu joints after S–S electromigration with the current density of 1.0 × 10^4 A/cm^2 at 70 °C for different times, with magnified view of the cathode side and the anode side: **a**–**c** 25 h, **d**–**f** 50 h, **g**–**i** 100 h, **j**–**l** 200 h

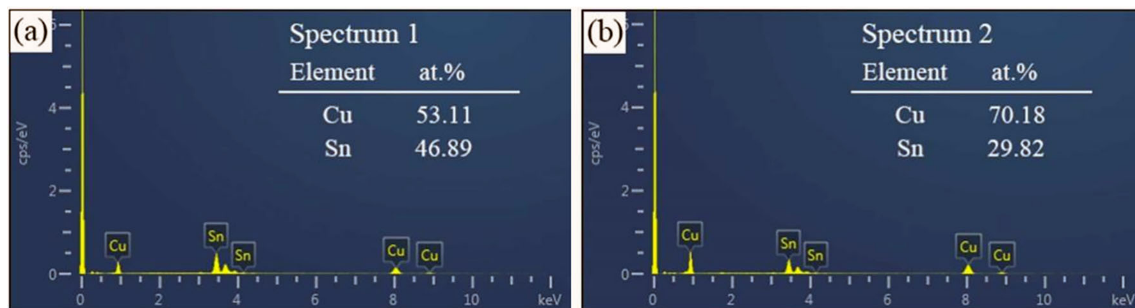

Fig. 5 Results of EDS analysis of interfacial IMCs in the Cu/Sn-58Bi/Cu joint shown in Fig. 4k: **a** Spectrum 1, **b** Spectrum 2

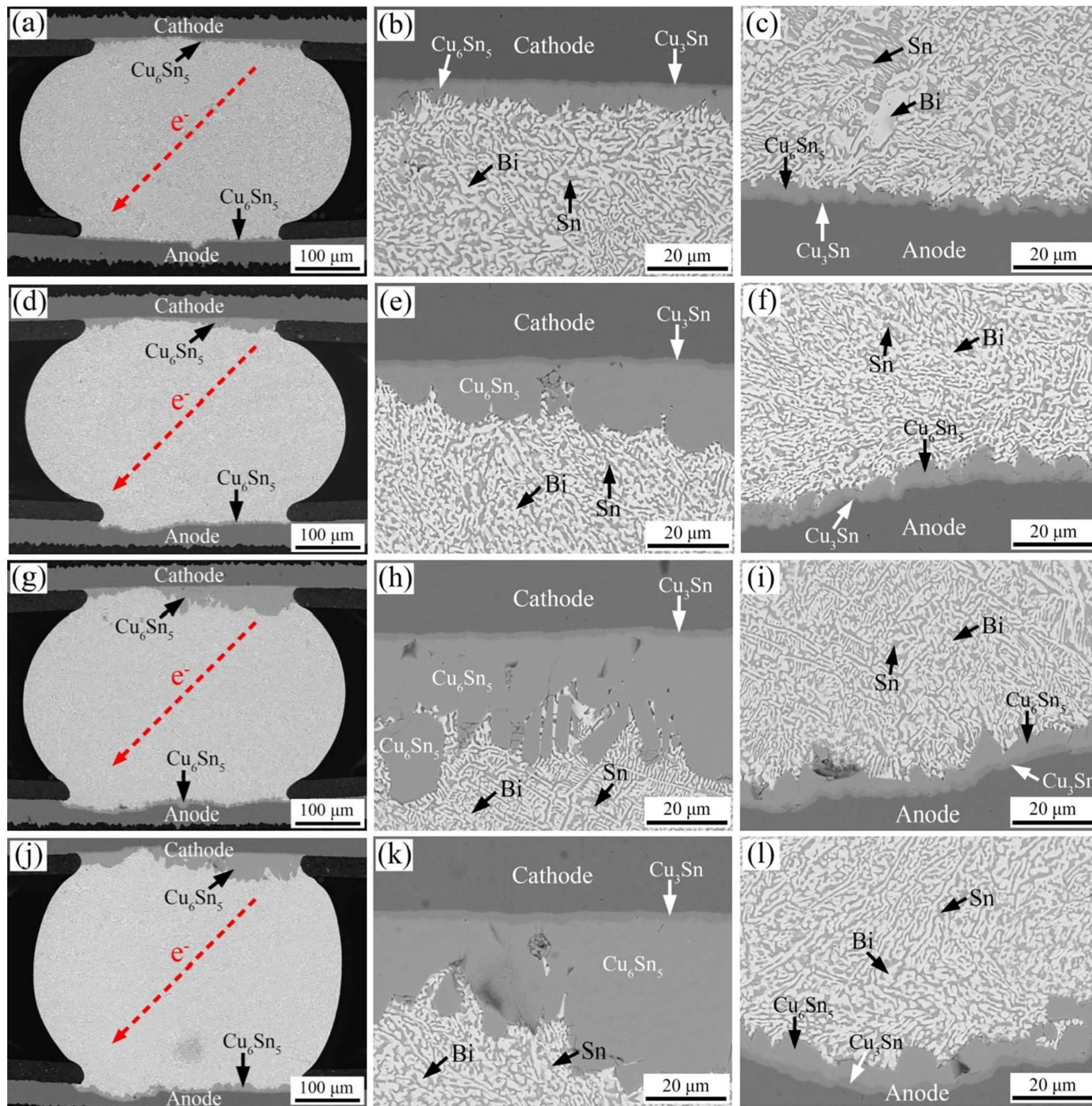

Fig. 6 Cross-sectional microstructures of BGA structure Cu/Sn-58Bi/Cu joints after S–S electromigration with the current density of 1.0 × 10^4 A/cm^2 at 135 °C for different times, with magnified view of the cathode side and the anode side: **a**–**c** 6 h, **d**–**f** 12 h, **g**–**i** 18 h, **j**–**l** 25 h

interfacial IMCs on both the cathode and anode sides are about 6.81 μm and 4.74 μm, respectively. Besides, Cu substrate in local area on the anode side dissolves into the solder. As the current stressing time increases to 12 h, as depicted in Fig. 6d–f, the thicknesses of the interfacial IMCs on both the cathode and anode sides further increase to 11.62 μm and 5.55 μm, respectively. Moreover, more Cu substrate in local area on the anode side dissolves into the solder. When the current stressing time reaches to 18 h and to 25 h, as shown in Fig. 6g–l, the thickness of the interfacial IMCs on the cathode side increases significantly to 27.58 μm and finally to 29.22 μm, respectively, while that on the anode side increases slightly to 5.96 μm and finally to 8.52 μm, respectively. Besides, the dissolution of Cu substrate in local area on the anode side is aggravated, resulting in the irregular interface. Moreover, the morphology of the interfacial Cu_6Sn_5 layer on the cathode side changes from scallop-type to the combination of scallop-type and rod-type, while that on the anode side remains scallop-type.

In addition, it is worth noting that the electric current crowding effect and the Joule heating effect

occur easily near the top right and bottom left of joint due to the geometrically asymmetric structure of BGA solder joint, therefore, the thickness of the interfacial IMCs near the top right corner is significant thicker than that in other regions, as shown in Fig. 4a, d, g, and j. Moreover, it is interesting to find that Bi atoms do not accumulate to form a continuous Bi-rich layer on the anode side during S–S electromigration at 135 °C, as shown in Fig. 6a, d, g, and j, which is different from the result of the joints under S–S electromigration at 70 °C shown in Fig. 4. According to the result reported in a previous study [12], as the Bi concentration of chemical gradient exceeds the Bi flux driven by electronic wind force in the molten Sn-58 solder joint, the Bi atoms on the anode side will reversely diffuse into the solder against the electron flow moving direction, then the Bi-rich layer on the anode side dissolves into the solder. Therefore, in this study, the reason for the disappearance of Bi-rich layer on the anode side maybe attributed to the increasing temperature by Joule heating effect, which causes the solder joints reach their melting point, and the Bi atoms on the anode side reversely diffuse into the solder until the Bi-rich layer is completely dissolved into the solder.

3.3 The microstructural evolution of solder joints during L–S electromigration

Figure 7 shows the cross-sectional microstructures of BGA structure Cu/Sn-58Bi/Cu joints after L–S electromigration with the current density of 1.0×10^4 A/cm^2 at 150 °C for different times. During L–S electromigration at 150 °C, which the temperature is higher than the melting temperature of Sn-58Bi solder, the solder remains liquid state. Comparing with solder joints undergoing S–S electromigration shown in Fig. 4 and 6, distinct differences have been observed under L–S electromigration. For example, after current stressing for 6 h, as shown in Fig. 7a–c, a thicker planar-type Cu_3Sn layer forms at the interface between the Cu_6Sn_5 layer and Cu substrate, and the thicknesses of the interfacial IMCs on both the cathode and anode sides increase to 6.57 μm and 11.92 μm, respectively. Beside, some interfacial Cu_6Sn_5 grains and part of Cu substrate on the cathode side dissolve into the molten solder. As the current stressing time increases to 12 h, as depicted in Fig. 7d–f, the thickness of the interfacial IMCs on the cathode side increases slightly to 8.65 μm, while that on the anode side increases significantly to 19.32 μm, and the morphology of the interfacial Cu_6Sn_5 layer on the cathode side remains scallop-type, while that on the anode side changes from the scallop-type to the combination of scallop-type and nod-type. In addition, the dissolution of Cu substrate on the cathode side is aggravated. As the current stressing time increases to 18 h, as shown in Fig. 7g–i, the thickness of the interfacial IMCs on the cathode side decreases slightly to 8.10 μm due to the local dissolution of interfacial IMCs, while that on the anode side further increases obviously to 28.19 μm. Besides, the morphology of the interfacial Cu_6Sn_5 layer on the cathode side remains scallop-type, while that on the anode side changes completely into nod-type. In addition, the dissolution of Cu substrate on the cathode side is further aggravated. Finally, when the current stressing time increases to 25 h, as shown in Fig. 7j–l, the interfacial IMCs and the Cu substrate on the cathode side are almost completely dissolved, and the interfacial IMCs on the anode side grows significantly, which its thickness increases to 77.65 μm. It is worth noting that during L–S electromigration at 150 °C, there is no Bi-rich layer on the anode side, as shown in Fig. 7a, d, g, and j. This is because the driving force generated by chemical potential exceeds that generated by electronic wind, which makes the Bi atoms on the anode side diffuse back into the solder until the Bi-rich layer is completely dissolved into the solder.

In order to clarify the effect of the current density on the interfacial behavior in molten solder, we carried out the L–S electromigration at 150 °C, which the current density is 1.5×10^4 A/cm^2, and the results are shown in Fig. 8. Obviously, current density plays an important role in the interfacial behavior in molten solder. For example, after current stressing for 6 h, as shown in Fig. 8a–c, most of the interfacial IMCs and Cu substrate on the cathode side dissolve into the molten solder, while the interfacial Cu_6Sn_5 on the anode side grows significantly into the molten solder, resulting in the thickness of the interfacial IMCs on the anode side increases dramatically to 60.64 μm, and the morphology of the interfacial Cu_6Sn_5 layer on the anode side changes from scallop-type to rod-type. Meanwhile, the thickness of the interfacial Cu_3Sn layer on the anode side increases obviously. As the current stressing time increases to 12 h, as depicted in Fig. 8d–f, the dissolution of interfacial IMCs and Cu substrate on the cathode side is more severe, and the thickness of interfacial IMCs on the anode side

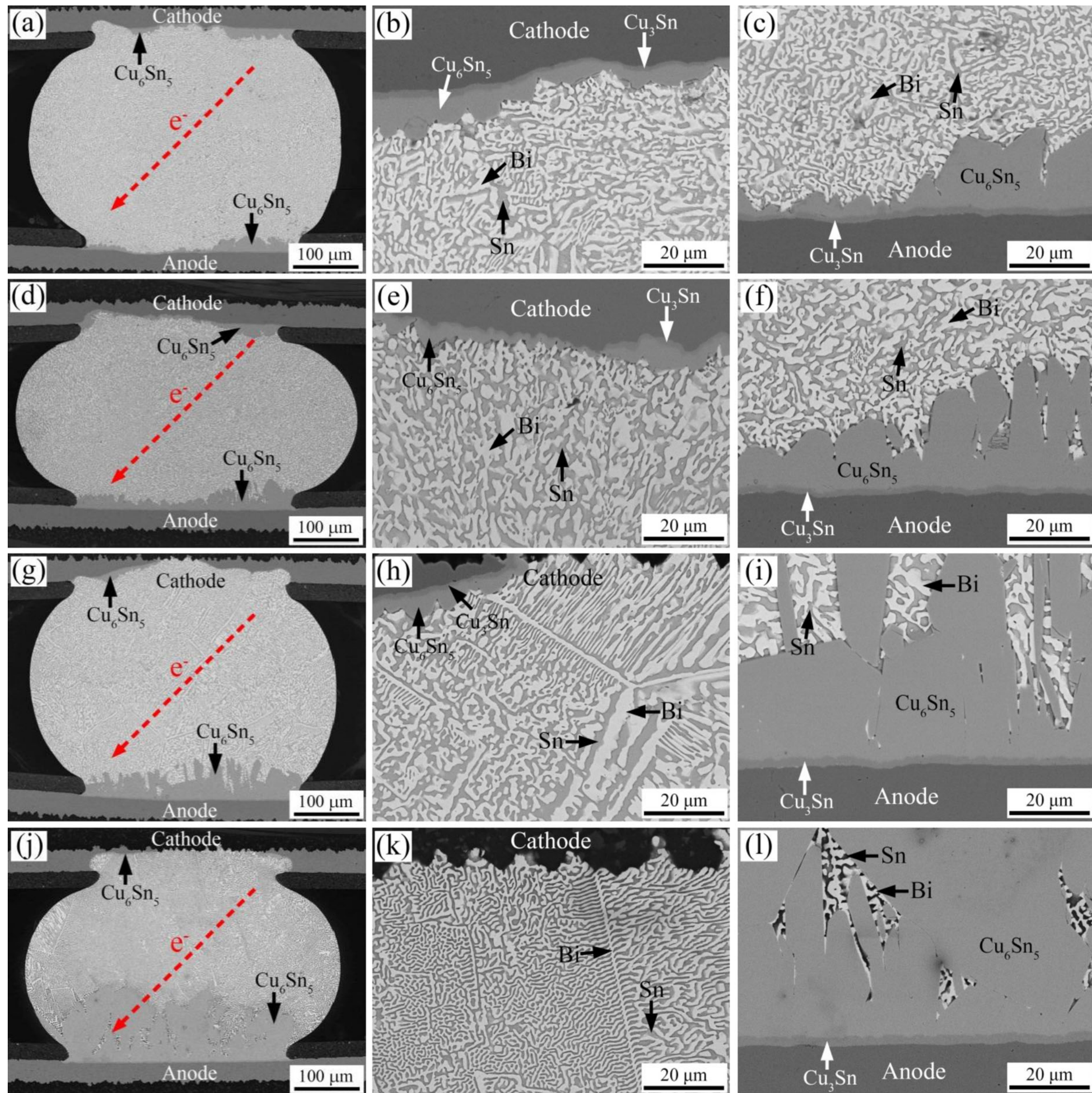

Fig. 7 Cross-sectional microstructures of BGA structure Cu/Sn-58Bi/Cu joints after L–S electromigration with the current density of 1.0 × 10^4 A/cm^2 at 150 °C for different times, with magnified view of the cathode side and the anode side: **a**–**c** 6 h, **d**–**f** 12 h, **g**–**i** 18 h, **j**–**l** 25 h

increases to 65.03 μm, and the structure of interfacial IMCs on the anode side becomes more compact. When the current stressing time further increases to 18 h, as shown in Fig. 8g–i, it is obviously to observe that the interfacial IMCs and Cu substrate on the cathode side are completely dissolved into the molten solder. Besides, the morphology of the interfacial Cu_6Sn_5 layer on anode side changes from rod-type to planar-type, and the thickness of interfacial IMCs on the anode side further increases to 72.89 μm. Moreover, a number of Bi-rich precipitates appear in the solder. The reason for the formation of Bi-rich precipitates could be attributed to the increasing Bi content in solder due to the consumption of Sn in Cu-Sn interfacial reaction. When the joint sample cools down and solidifies, Bi begins to precipitate in the formation of Bi-rich phases. It is worth noting that these massive Bi-rich precipitates could seriously deteriorate the bonding strength of solder joint [30]. When the current stressing time further increases to 25 h, as shown in Fig. 8j–l, comparing with results shown in Fig. 8g–i, there is little change in the

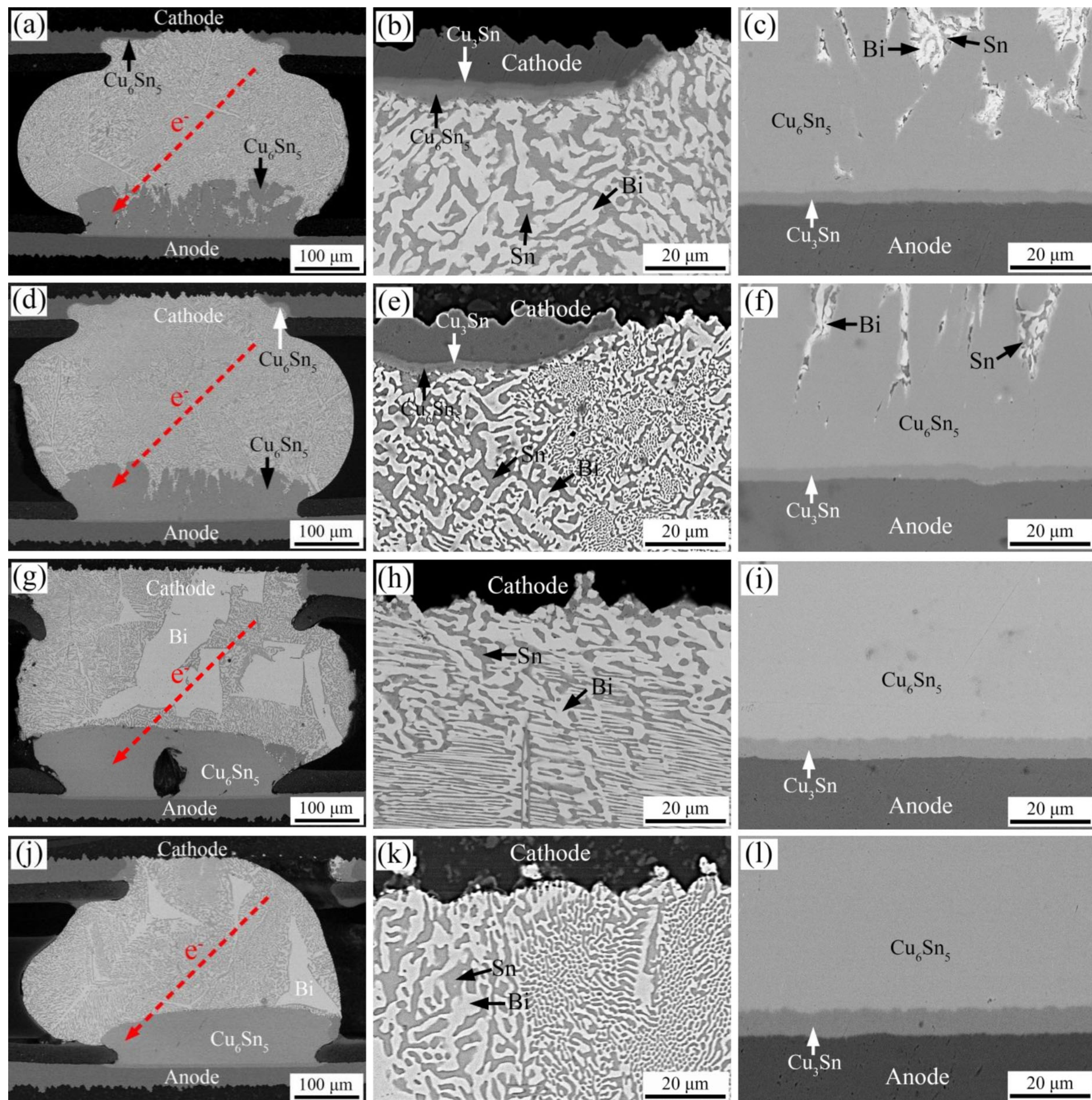

Fig. 8 Cross-sectional microstructures of BGA structure Cu/Sn-58Bi/Cu joints after L–S electromigration with the current density of 1.5×10^4 A/cm^2 at 150 °C for different times, with magnified view of the cathode side and the anode side: **a**–**c** 6 h, **d**–**f** 12 h, **g**–**i** 18 h, **j**–**l** 25 h

morphology of interfacial Cu_6Sn_5 layer and the thickness of the interfacial IMCs on the anode side due to the limitation of Cu atoms diffusing from Cu substrate on the cathode side, nevertheless, the thickness of the planar-type Cu_3Sn layer on the anode side increases significantly to 7.14 μm, resulting from the transformation of interfacial Cu_6Sn_5 during L–S electromigration at 150 °C.

Figure 9 shows the cross-sectional microstructures of BGA structure Cu/Sn-58Bi/Cu joints after L–S electromigration with the current density of 1.0×10^4 A/cm^2 at 170 °C for different times. During L–S electromigration at 170 °C, which the temperature is much higher than the melting temperature of Sn-58Bi solder, the solder also remains liquid state. After current stressing for 6 h, as shown in Fig. 9a–c, the interfacial Cu_6Sn_5 layer with morphology of rod-type grows into the molten solder, and a planar-type Cu_3Sn layer forms remarkably at the interface between the Cu_6Sn_5 layer and Cu substrate, and the

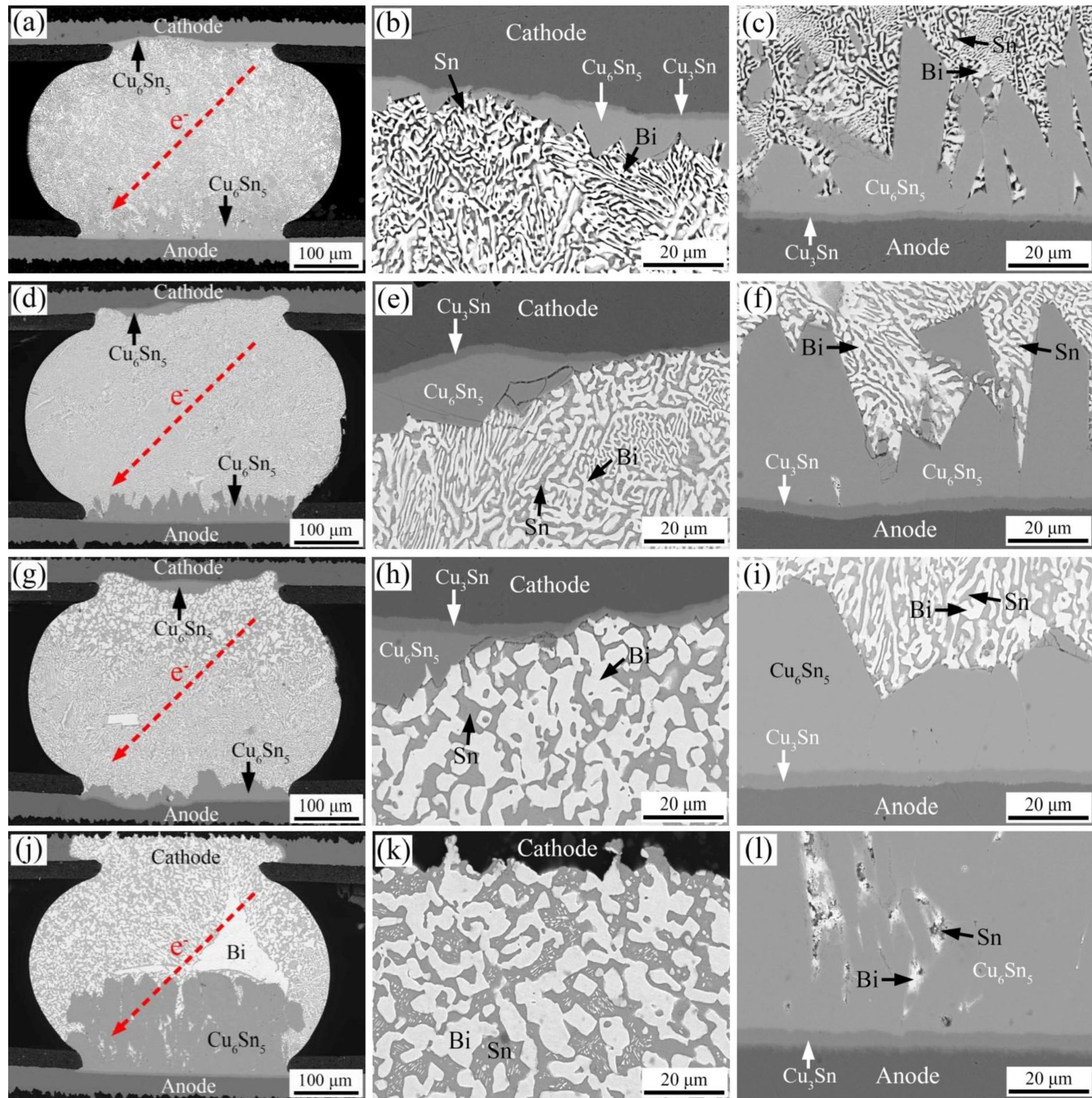

Fig. 9 Cross-sectional microstructures of BGA structure Cu/Sn-58Bi/Cu joints after L–S electromigration with the current density of 1.0 × 10^4 A/cm^2 at 170 °C for different times, with magnified view of the cathode side and the anode side: **a**–**c** 6 h, **d**–**f** 12 h, **g**–**i** 18 h, **j**–**l** 25 h

thicknesses of the interfacial IMCs on both the cathode and anode sides increase significantly to 4.30 μm and 26.65 μm, respectively. Meanwhile, part of the Cu substrate on the cathode side dissolves into the molten solder. As the current stressing time increases to 12 h, as depicted in Fig. 9d–f, the thicknesses of interfacial IMCs on both the cathode and anode sides further increase to 4.61 μm and 32.01 μm, respectively. In addition, the dissolution of Cu substrate on the cathode side is aggravated. As the current stressing time increases to 18 h, as shown in Fig. 9g–i, the thicknesses of the interfacial IMCs on both the cathode and anode sides further increase to 7.35 μm and 36.16 μm, respectively, and the dissolution of Cu substrate on the cathode side is further aggravated. When the current stressing time is up to 25 h, as shown in Fig. 9j–l, it is clearly to observe that the interfacial IMCs and Cu substrate on the cathode side are completely dissolved into the solder, in which a large number of Cu atoms diffuse to the anode side

and participate in the interfacial reaction between Cu and Sn, resulting in the dramatically growth of interfacial Cu_6Sn_5 layer on the anode side. Therefore, the thickness of interfacial IMCs on the cathode side decreases to 0 μm, while that on the anode side increases significantly to 119.50 μm. Furthermore, large Bi-rich phases also precipitate in the solder, resulting from the increasing Bi content in solder due to the consumption of Sn in Cu-Sn interfacial reaction.

3.4 Growth mechanism of the interfacial IMCs during S–S and L–S electromigration

Figure 10 reveals the variation of thicknesses of the interfacial IMCs of BGA structure Cu/Sn-58Bi/Cu joints during electromigration, which the total thickness of the IMCs is the sum of Cu_6Sn_5 and Cu_3Sn. The data points in Fig. 10 are presented as averages and ranges; some error bars are not visible because the range is smaller than the size of the data points. Clearly, during S–S electromigration at 70 °C and 135 °C, which the temperatures are lower than the melting temperature of Sn-58Bi solder, the thicknesses of interfacial IMCs on both the cathode and anode sides increase with prolonging the stressing time, and the thickness of interfacial IMCs on the cathode side is obvious thicker than that on the anode side, indicating that the current stressing induces a reverse polarity effect on the growth of interfacial IMCs during S–S electromigration, that is, current stressing significantly promotes the growth of interfacial IMCs on the cathode side, while reversely on the anode side, as demonstrated in Fig. 10a and b. Nevertheless, the growth behavior of the interfacial IMCs of joints during L–S electromigration is different from that during S–S electromigration, that is, during L–S electromigration at 150 °C and 170 °C, which the temperatures are higher than the melting temperature of Sn-58Bi solder, the thickness of interfacial IMCs on the anode side increases with extending the stressing time, while that on the cathode side increases firstly and then decreases with increasing the stressing time, and the thickness of interfacial IMCs on the anode side is significant thicker than that on the cathode side, indicating that the current stressing induces a polarity effect on the growth of interfacial IMCs during L–S electromigration, which the current stressing markedly promotes the growth of interfacial IMCs on the anode side, while reversely on the cathode side, as shown in Fig. 10c, d, and e. Thus, as the temperature increases from 70 to 170 °C, the physical state of the Sn-58Bi solder changes from solid to liquid state, and meanwhile the growth mechanism of the interfacial IMCs changes from the reverse polarity effect to the polarity effect during electromigration. In addition, the higher the current density and temperature, the more obvious the polarity effect, as depicted in Fig. 10c, d, and e.

Generally, the atomic diffusion flux during electromigration is mainly influenced by the combination of electronic wind force and chemical potential gradient as well as back stress [31]. However, the influence caused by back stress could be neglected in the present study because the threshold length on back stress to perform effectively must be lower than 15 μm [32]. In addition, during L–S electromigration in molten Sn-58Bi solder, the back stress is absented in liquid metal [12]. Therefore, the atomic diffusion flux during electromigration is dominated by the combination of electronic wind force and chemical potential, which can be expressed as follows [31]:

$$J = J_{em} + J_{chem} = \left({}^{CD}/_{kT} \right) \rho j Z^* e - D \left({}^{\partial C}/_{\partial x} \right) \quad (1)$$

where J_{em} is the flux caused by the electronic wind force, J_{chem} is the flux caused by the chemical potential gradient, C is atomic concentration, D is the diffusion coefficient of atoms, k is Boltzmann's constant, T is absolute temperature, ρ is resistivity of Sn-58Bi solder, j is current density, Z^* is the effective charge number, which negative effective charge number indicates that the atoms diffuse with the same direction of electron flow, i.e., from cathode to anode side, otherwise, positive value indicates the opposite direction of atoms. In addition, e is the electron charge, and $\partial C/\partial x$ is concentration gradient of diffusion atom, negative sign indicates the direction of diffusion is opposite to that of concentration gradient.

Figure 11 shows the schematic diagram of Cu atomic flux in BGA structure Cu/Sn-58Bi/Cu joints during S–S and L–S electromigration with the current density of 1.0×10^4 A/cm^2. According to the Eq. (1), the Cu atomic fluxes on both the cathode and anode sides can be obtained as follows:

$$J^{Cu}_{cathode} = J^{Cu}_{em1} + J^{Cu}_{chem1} - J^{Cu}_{em2} - J^{Cu}_{chem2} \quad (2)$$

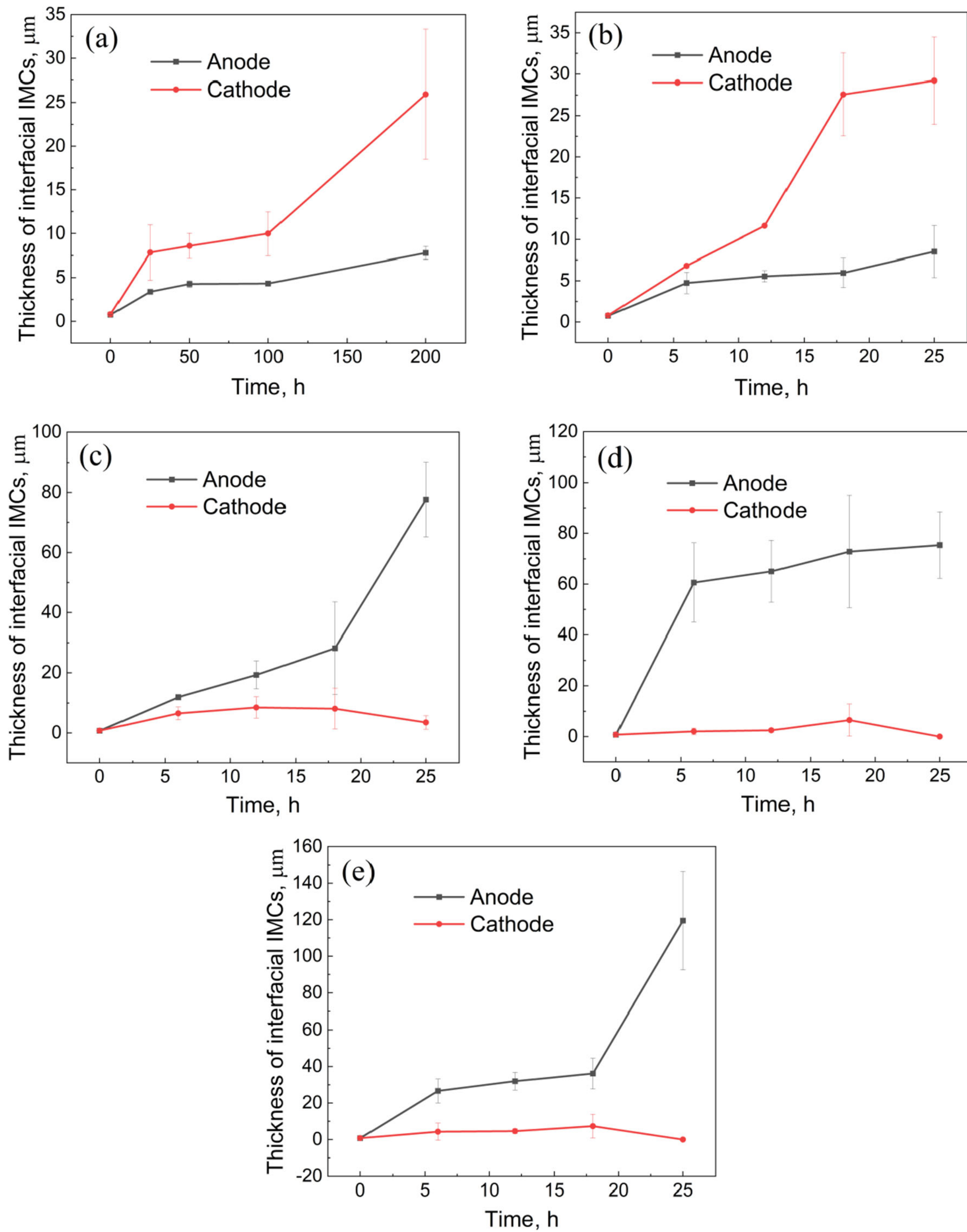

Fig. 10 Variation of thicknesses of the interfacial IMCs of BGA structure Cu/Sn-58Bi/Cu joints stressed with different current densities: **a** S–S electromigration with the current density of 1.0×10^4 A/cm^2 at 70 °C, **b** S–S electromigration with the current density of 1.0×10^4 A/cm^2 at 135 °C, **c** L–S electromigration with the current density of 1.0×10^4 A/cm^2 at 150 °C, **d** L–S electromigration with the current density of 1.5×10^4 A/cm^2 at 150 °C, **e** L–S electromigration with the current density of 1.0×10^4 A/cm^2 at 170 °C

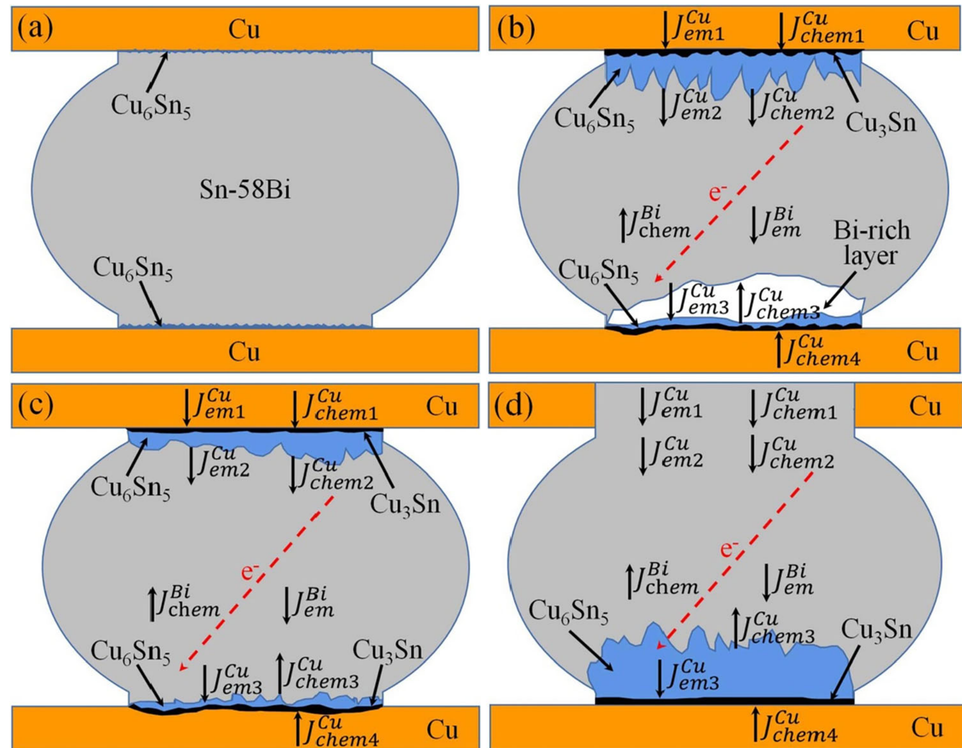

Fig. 11 Schematic diagram of both the Cu and Bi atomic fluxes in BGA structure Cu/Sn-58Bi/Cu joints during electromigration with the current density of 1.0 × 10^4 A/cm^2 at different temperatures: **a** Original state after reflow soldering, **b** S–S electromigration at temperature significantly lower than the melting temperature of Sn-58Bi solder, **c** S–S electromigration at temperature slightly lower than the melting temperature of Sn-58Bi, **d** L–S electromigration at temperature above the melting temperature of Sn-58Bi

$$J^{Cu}_{anode} = J^{Cu}_{em3} + J^{Cu}_{chem4} - J^{Cu}_{chem3} \quad (3)$$

According to Fig. 11 and Eqs. (2, 3), for the cathode side, the J^{Cu}_{em1} and J^{Cu}_{chem1} flow into the IMCs layer and lead to the interfacial IMCs getting thicker, while J^{Cu}_{em2} and J^{Cu}_{chem2} flow out the IMCs layer and result in the interfacial IMCs becoming thinning. For the anode side, the J^{Cu}_{em3} and J^{Cu}_{chem4} flow into the interfacial IMCs layer and lead to the interfacial IMCs getting thicker, while J^{Cu}_{chem3} flows out the interfacial IMCs layer and results in the interfacial IMCs becoming thinning.

Therefore, as shown in Fig. 11b, during S–S electromigration at temperature significantly lower than the melting temperature of Sn-58Bi solder, on the cathode side, under the combined effect of electronic wind force and chemical potential, a large amount of Cu atoms from substrate diffuse to the Sn-58Bi/Cu interface, and react with Sn atoms from Sn-58Bi solder to form the interfacial IMCs, which leads to the decrease of J^{Cu}_{em2} and J^{Cu}_{chem2}, as a result, $J^{Cu}_{em1} + J^{Cu}_{chem1} > J^{Cu}_{em2} + J^{Cu}_{chem2}$, and the thickness of interfacial IMCs increases with prolonging the stressing time. On the anode side, similarly, due to the formation of interfacial IMCs, $J^{Cu}_{chem4} > J^{Cu}_{chem3}$, meanwhile, the Cu atoms are driven continuously to the Sn-58Bi/Cu interface by electronic wind force, which the driving force of electronic wind may be larger than the chemical potential, therefore, $J^{Cu}_{em3} + J^{Cu}_{chem4} > J^{Cu}_{chem3}$, and the thickness of interfacial IMCs increases with increasing the stressing time. However, because the Bi-rich layer on the anode side can act as a diffusion barrier and restrain the diffusion of Cu atoms when it becomes thick enough [33], the thickness of interfacial IMCs on the cathode side is much thicker than that on the anode side, in other words, a reverse polarity effect occurs in the growth mechanism of interfacial IMCs.

As depicted in Fig. 11c, during S–S electromigration at temperature slightly lower than the melting temperature of Sn-58Bi solder, because the electrical resistivity of Sn-58Bi solder ranges from 30 to 40 μΩ cm, while that of Bi and Sn are 115 μΩ cm and 11.4 μΩ cm, respectively [17], when the Bi-rich layer forms on the anode side, the joule heat and the temperature on the anode side will increase due to the high electrical resistivity of Bi, as a result, there will be a local melting phenomenon of Sn-58Bi solder on the anode side, and the diffusion rate of Cu atoms on the anode side increases. However, inequalities are still exists, i.e., $J^{Cu}_{em1} + J^{Cu}_{chem1} > J^{Cu}_{em2} + J^{Cu}_{chem2}$, and $J^{Cu}_{em3} + J^{Cu}_{chem4} > J^{Cu}_{chem3}$. Therefore, the thicknesses of interfacial IMCs on both the cathode and anode sides increase with

prolonging the stressing time, and the thickness of interfacial IMCs on the cathode side is thicker than that on the anode side, and a reverse polarity effect occurs in the growth mechanism of interfacial IMCs.

As demonstrated in Fig. 11d, during L–S electromigration at temperature above the melting temperature of Sn-58Bi solder, on the cathode side, at the early state of electromigration process, the formation of interfacial IMCs consumes partial Cu atoms, which leads to $J_{em1}^{Cu} + J_{chem1}^{Cu} > J_{em2}^{Cu} + J_{chem2}^{Cu}$, as a result, the thickness of interfacial IMCs increases firstly with extending the stressing time. Nevertheless, since the diffusion rate of Cu atoms in the molten solder is much faster than that in the solid Cu_6Sn_5 layer [34, 35], Cu atoms on the cathode side migrate quickly to the anode side under the effect of electronic wind force, and react with Sn atoms from solder to form Cu_6Sn_5 layer, as a result, not only $J_{em1}^{Cu} < J_{em2}^{Cu}$, but also decreases the Cu concentration in front of the Sn-58Bi/Cu interface on the cathode side and correspondingly increases J_{chem2}^{Cu}. Therefore, $J_{em1}^{Cu} + J_{chem1}^{Cu} < J_{em2}^{Cu} + J_{chem2}^{Cu}$, and the interfacial IMCs on the cathode side begins to decompose, and then the thickness of interfacial IMCs decreases until zero with prolonging the stressing time. On the anode side, since the electronic wind force plays a dominant role in the migration of Cu atoms from the cathode side to the anode side, $J_{em3}^{Cu} + J_{chem4}^{Cu} > J_{chem3}^{Cu}$. Thus, the thickness of interfacial IMCs increases continuously with extending the stressing time. Therefore, during L–S electromigration, the thickness of interfacial IMCs on the anode side is much larger than that on the cathode side, in other words, a polarity effect occurs in the growth mechanism of interfacial IMCs.

3.5 Growth mechanism of Bi-rich layer during S–S and L–S electromigration

Figure 11 also demonstrates the schematic diagram of Bi atomic flux in BGA structure Cu/Sn-58Bi/Cu joints during electromigration with the current density of 1.0 × 10^4 A/cm^2. According to the Eq. (1), the Bi atomic flux on the anode side can be given as follow:

$$J_{anode}^{Bi} = J_{em}^{Bi} - J_{chem}^{Bi} \tag{4}$$

Therefore, as shown in Fig. 11b, during S–S electromigration at temperature significantly lower than the melting temperature of Sn-58Bi solder, due to the original homogeneous microstructure of Sn-58Bi solder shown in Fig. 3 and Fig. 11a, there is no Bi concentration gradient in joint, and electronic wind force plays a dominant role in Bi atomic diffusion flux, thus, $J_{em}^{Bi} > J_{chem}^{Bi}$, Bi atoms continuously migrate and accumulate to form a Bi-rich layer on the anode side with increasing the stressing time.

As indicated in Fig. 11c, during S–S electromigration at temperature slightly lower than the melting temperature of Sn-58Bi solder, as mentioned above, due to the higher electrical resistivity of Bi than that of the Sn-58Bi solder, when the Bi-rich layer forms on the anode side under the effect of electronic wind force, the joule heat and temperature near the Bi-rich layer will increase, which leads to local melting of solder in front of the Bi-rich layer and correspondingly the increase of diffusion rate of Bi atoms. As a result, the driving force generated by chemical potential increases and exceeds that generated by electronic wind, i.e., $J_{em}^{Bi} < J_{chem}^{Bi}$, and the Bi atoms on the anode side diffuse back into the solder until the Bi-rich layer is completely dissolved into the solder.

As depicted in Fig. 11d, during L–S electromigration at temperature above the melting temperature of Sn-58Bi solder, the Sn-58Bi solder remains liquid state, similarly, since the diffusion rate of Bi atoms in the molten solder is much faster than that in the solid solder, the driving force generated by chemical potential exceeds that generated by electronic wind, i.e., $J_{em}^{Bi} < J_{chem}^{Bi}$, and the Bi atoms on the anode side reversely diffuse into the solder, eventually leading to the disappearance of Bi-rich layer. It should be mentioned that with the increase of the distance away from the interface between the Sn-58Bi solder and Bi-rich layer, the driving force generated by chemical potential decreases gradually, and its value on the cathode side is smaller than that generated by electronic wind. Therefore, Bi atoms do not accumulate to produce a Bi-rich layer on both the anode and cathode sides.

4 Conclusion

In this study, the growth mechanisms of IMCs and Bi-rich layer of the BGA structure Cu/Sn-58Bi/Cu joints under during S–S electromigration in solid solder and L–S electromigration in molten solder

were comprehensively investigated. The following conclusions can be drawn:

(1) During S–S electromigration at temperature significantly lower than the melting temperature of Sn-58Bi solder, current stressing induces a reverse polarity effect on the growth of interfacial IMCs, i.e., the interfacial IMCs on the cathode side is thicker than that on the anode side. Under the effect of electronic wind force, Bi atoms migrate and accumulate to form a continuous Bi-rich layer on the anode side.

(2) During S–S electromigration at temperature slightly lower than the melting temperature of Sn-58Bi solder, current stressing causes a reverse polarity effect on the growth of interfacial IMCs. The local melting of solder occurs on the anode side due to the Joule heating effect, the Bi atoms on the anode side reversely diffuse into the solder, eventually leading to the disappearance of Bi-rich layer.

(3) During L–S electromigration at temperature above the melting temperature of Sn-58Bi solder, current stressing causes a polarity effect on the growth of interfacial IMCs, i.e., the interfacial IMCs on the anode side is thicker than that on the cathode side. The higher the current density and temperature, the more obvious the polarity effect. Bi atoms do not migrate and accumulate to form a continuous Bi-rich layer on the anode side.

(4) The transition in growth mechanism of interfacial IMCs from the reverse polarity effect to the polarity effect in BGA structure Cu/Sn-58Bi/Cu joints is attributed to the combined effect of the electronic wind force flux (J_{em}) and the chemical potential gradient flux (J_{chem}).

Author contributions

JH: Conceptualization, Methodology, Formal analysis, Data curation, Writing – original draft. XW: Methodology, Experiment, Data curation, Writing – original draft. JC: Methodology, Experiment. WW: Methodology, Experiment. YZ: Writing, Review & Editing. FL: Formal analysis, Supervision. BQ: Formal analysis, Supervision. HW: Formal analysis, Supervision.

Funding

This research was funded by the Natural Science Foundation of Guangxi Province (Grant Nos. AD19245093 and 2019GXNSFAA245059), Middle-aged and Young Teachers' Basic Ability Promotion Project of Guangxi (Grant No. 2019KY0221), GDAS Special Project of Science and Technology Development (Grant Nos. 2020GDASYL-20200402006 and 2022GDASZH-2022010109), and National Key Research and Development Program of China (Grant No. 2020YFE0205300).

Data availability

The data and materials that support the findings of this study are available from the corresponding author upon reasonable request. The data are not publicly available as the data also forms part of an ongoing study.

Declarations

Conflict of interest The authors declare that they have no known competing financial interests or personal relationships that could have appeared to influence the work reported in this paper.

Ethical approval This article does not contain any studies with human tissues or animals performed by any of the authors.

Consent to participate This research is not related to human subjects.

References

1. J.A. Depiver, S. Mallik, E.H. Amalu, Eng. Fail. Anal. **125**, 105447 (2021)
2. K.M. Chu, C.S. Lee, S.H. Park, Y.C. Sohn, Microelectron. Reliab. **75**, 53 (2017)
3. F.J. Wang, L.T. Liu, M.F. Wu, D.Y. Li, J. Mater. Sci. Mater. Electron. **29**, 8895 (2018)
4. Y.L. Chen, J.Y. Jia, H.Z. Fu, Z. Zeng, Int. J. Fatigue **87**, 216 (2016)
5. Y. Ma, X.Z. Li, L.Z. Yang, W. Zhou, M.X. Wang, W.B. Zhu, P. Wu, Mater. Sci. Eng. A **696**, 437 (2017)
6. S.B. Liang, C.B. Ke, J.Q. Huang, M.B. Zhou, X.P. Zhang, Microelectron. Reliab. **92**, 1 (2019)

7. N. Jiang, L. Zhang, L.L. Gao, W.M. Long, S.J. Zhong, L. Zhang, J. Mater. Sci. Mater. Electron. **32**, 16970 (2021)
8. K.D. Min, K.H. Jung, C.J. Lee, B.U. Hwang, S.B. Jung, J. Alloys Compd. **857**, 157595 (2021)
9. Y.X. Liu, Y.C. Chu, K.N. Tu, Acta Mater. **117**, 146 (2016)
10. H.B. Qin, T.H. Liu, W.Y. Li, W. Yue, D.G. Yang, Microelectron. Reliab. **115**, 113995 (2020)
11. M.L. Huang, Q. Zhou, N. Zhao, X.Y. Liu, Z.J. Zhang, J. Mater. Sci. **49**, 1755 (2014)
12. F.J. Wang, H. Chen, D.Y. Li, Z.J. Zhang, X.J. Wang, Electron. Mater. Lett. **15**, 36 (2019)
13. Z.J. Zhang, M.L. Huang, Acta. Metall. Sin. **56**, 1386 (2020)
14. X. Gu, K.C. Yung, Y.C. Chan, J. Mater. Sci. Mater. Electron. **21**, 1090 (2010)
15. D.L. Ma, P. Wu, Mater. Sci. Eng. A **651**, 499 (2016)
16. J.Q. Huang, M.B. Zhou, X.P. Zhang, J. Electron. Mater. **46**, 1504 (2017)
17. T. Siewert, S. Liu, D.R. Smith, J.C. Madeni, in Properties of Lead-Free Solders (2002)
18. Z. Wang, Q.K. Zhang, Y.X. Chen, Z.L. Song, J. Mater. Sci. Mater. Electron. **30**, 18524 (2019)
19. S.M. Lee, J.W. Yoon, S.B. Jung, J. Mater. Sci. Mater. Electron. **27**, 1105 (2015)
20. F. Guo, Q. Liu, L.M. Ma, Y. Zuo, J. Mater. Res. **31**, 1793 (2016)
21. S.B. Liang, C.B. Ke, C. Wei, J.Q. Huang, M.B. Zhou, X.P. Zhang, J. Mater. Res. **34**, 2775 (2019)
22. J.R. Huang, C.M. Tsai, Y.W. Lin, C.R. Kao, J. Mater. Res. **23**, 250 (2008)
23. H.T. Ma, A. Kunwar, J.H. Sun, B.F. Guo, H.R. Ma, Scr. Mater. **107**, 88 (2015)
24. Z.J. Zhang, M.L. Huang, Acta. Metall. Sin. **52**, 592 (2017)
25. X.M. Li, F.L. Sun, H. Zhang, M. Liu, R. Fan, J. Alloys Compd. **739**, 388 (2018)
26. J.Q. Huang, M.B. Zhou, S.B. Liang, X.P. Zhang, J. Mater. Sci. Mater. Electron. **29**, 7651 (2018)
27. C.M. Chen, L.T. Chen, Y.S. Lin, J. Electron. Mater. **36**, 168 (2007)
28. H.F. Zou, Q.K. Zhang, Z.F. Zhang, Mater. Sci. Eng. A **532**, 167 (2012)
29. X. Zhao, M. Saka, M. Muraoka, M. Yamashita, H. Hokazono, J. Electron. Mater. **43**, 4179 (2014)
30. J. Shen, Y.Y. Pu, H.G. Yin, D.J. Luo, J. Chen, J. Alloys Compd. **614**, 63 (2014)
31. H. Gan, K.N. Tu, J. Appl. Phys. **97**, 063514 (2005)
32. C.C. Wei, C. Chen, J. Appl. Phys. **88**, 182105 (2006)
33. X. Gu, D. Yang, Y.C. Chan, B.Y. Wu, J. Mater. Res. **23**, 2591 (2008)
34. B. Chao, S.H. Chae, X.F. Zhang, K.H. Lu, J. Im, P.S. Ho, Acta Mater. **55**, 2805 (2007)
35. P. Kumar, J. Howarth, I. Dutta, J. Appl. Phys. **115**, 044915 (2014)

Publisher's Note Springer Nature remains neutral with regard to jurisdictional claims in published maps and institutional affiliations.